J. Sustain. Metall. (2017) 3:846–857
https://doi.org/10.1007/s40831-017-0148-y

RESEARCH ARTICLE

Pyrometallurgical Treatment of Apatite Concentrate with the Objective of Rare Earth Element Recovery: Part II

Mark William Kennedy[1] · Tianming Sun[2] · Lourdes Yurramendi[3] · Sander Arnout[4] · Ragnhild E. Aune[1] · Gabriella Tranell[1]

Published online: 28 November 2017

Abstract Apatite, $Ca_5(PO_4)_3F$, is a useful raw material for the production of both elemental phosphorus and phosphoric acid, and the mine tailings present at Luossavaara-Kiirunavaara AB (LKAB) in Kiruna, Sweden, represent a significant potential European source of apatite if upgraded to a concentrate. In the present study, pilot apatite concentrate made from the LKAB tailings has been pyrometallurgically treated using carbon to extract phosphorus without fluxing at temperatures exceeding 1800 °C, with the ultimate objective of recovery of rare earth elements (REEs) from the resulting slag/residue phases. Experimental behavior has been modeled using equilibrium thermodynamic predictions performed using HSC®. A process is proposed, and mass–energy balance presented, for the simultaneous production of P_4 and CaC_2 (ultimately for acetylene, C_2H_2, and PVC production) from apatite, producing a lime residue significantly enriched in REEs. Possible implications to kiln-based processing of apatite are also discussed.

The contributing editor for this article was Bernd Friedrich.

✉ Mark William Kennedy
mark.w.kennedy@ntnu.no

[1] Department of Materials Science and Engineering, Norwegian University of Science and Technology (NTNU), 7491 Trondheim, Norway

[2] Department of Materials Science and Engineering, Royal Institute of Technology (KTH), 100 44 Stockholm, Sweden

[3] TECNALIA Parque Tecnológico de San Sebastián, Mikeletegi Pasealekua, 2, 20009 Donostia-San Sebastián, Gipuzkoa, Spain

[4] InsPyro, Kapeldreef 60, 3001 Leuven, Belgium

Keywords Apatite · Rare earth · REE · Phosphorus · Smelting · Improved hard process · IHP

Introduction

Apatite is a common raw material both for the production of elemental phosphorus (P_4), as shown in Fig. 1, and for phosphorus pentoxide (P_2O_5), which is used primarily to produce phosphoric acid [1, 2]. One possible production route for both products is via carbothermic reduction of apatite [3]. The high energy consumption of the traditional Wöhler electric furnace pyrometallurgical route, e.g., reported for one furnace to be as high as 14.3 MWh/mt P_4 [4], places it at an economic disadvantage for phosphoric acid production in comparison to alternative processes such as the wet process. In the wet process, phosphoric acid is produced by the digestion of high-grade phosphate rock, e.g., apatite, using sulfuric acid, followed by filtration and subsequent vacuum concentration [5]. Presently, at least one enhanced thermal process, the Improved Hard Process (IHP), is therefore being commercialized [6, 7].

The magnetite iron ore type of the Luossavaara-Kiirunavaara AB (LKAB) mine at Kiruna, Sweden, is known to contain both apatite and significant quantities of Rare Earth Elements (REEs) within the apatite matrix [8], as well as within the monazite, allanite [9, 10], and titanite phases [11]. To serve as a raw material for one of the REE recovery studies conducted as part of the EU-sponsored "Recovery of Rare Earth Elements from Magnetic Waste in the WEEE Recycling Industry" (REEcover) project [12], the LKAB tailings containing 4–8% apatite were upgraded to apatite concentrate containing about 3500 ppm of REEs [9]. The chemical composition, and high-temperature behavior, of this concentrate has been

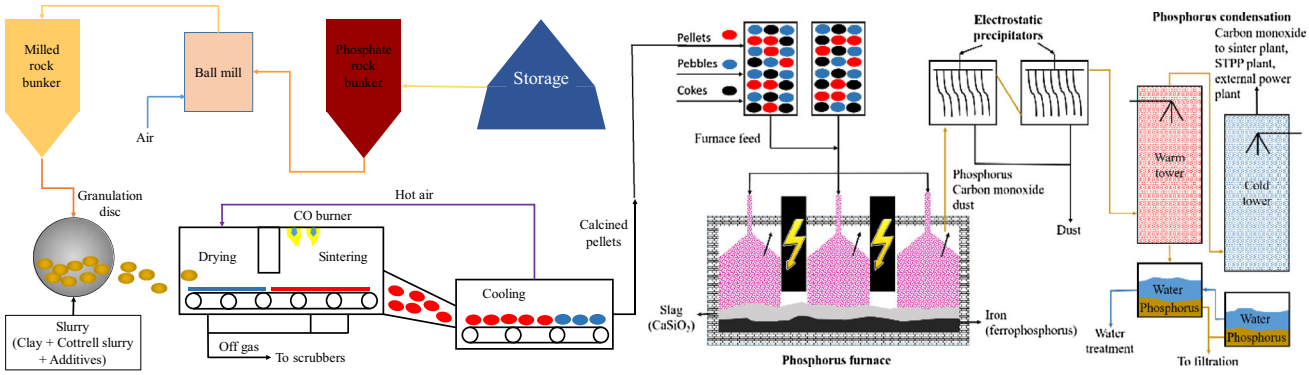

Fig. 1 The Wöhler process flowsheet for the production of P_4 from apatite concentrate [1] (color figure online)

characterized elsewhere, i.e., in Part I of the present article, where the impact of silicothermic reduction on the distribution of REEs was also studied [13].

In the present part of the article, i.e., Part II, the results of carbothermic phosphorus removal experiments will be presented, along with a simplified thermodynamic analysis and potential industrial implications of the research to both electric furnace and kiln-based processes. Extraction of phosphorus from apatite concentrate with and without iron addition has been studied, and the elemental distribution to gas, slag, and metal was estimated where possible. In addition, a process that could simultaneously produce both P_4 and CaC_2 is proposed and evaluated.

Phosphorus Extraction Experiments

Background

One drawback of silicothermic reduction of apatite, as discussed in Part I of this article, is the necessity of fluxing, which reduces or eliminates the potential to produce a slag with a higher rare earth concentration. It may also preclude the formation of desired high rare earth-containing phases for later physical separation and recovery [14]. One proven alternative for treating high-phosphorus feedstock is carbothermic reduction to make the so-called 'white' or 'yellow' phosphorus (P_4) [15]. Phosphate is also one of the EU's strategic raw materials [16]; therefore, the simultaneous production of P_4 and a high rare earth-containing slag can address two strategic materials issues simultaneously, while potentially generating much greater total value from the apatite resource.

In conventional carbothermic phosphorus production (as presented in Fig. 1), SiO_2 is used as a flux in order to achieve operating temperatures of the order of 1500 °C, and it produces a low-phosphorus slag (< 1 wt% P) [4], which should result in a similar outcome to the silicothermic extraction experiments presented in Part I of the present article, i.e., a low final concentration of REEs. Recently published work by Karshigina et al. [17] has disclosed a method using extremely concentrated nitric acid (due to the stability of the silicates) to recover REEs from high-silica discard slag produced as a by-product of the conventional carbothermic phosphorus process. The high-acid leach would seem to indicate difficulties in treating such slag, and the economics of such a process could be questioned particularly with the current low prices for REEs, as previously indicated in Fig. 1 of Part I of the article [13].

It is worth noting that the apatite concentrate used in the current study, having only ~ 2 wt% SiO_2 [10], is unusually pure with respect to a fluorapatite feedstock, which typically has 2–12 wt% SiO_2 [2]. Given that the concentrate in the absence of 'phosphate' is primarily CaO, the extremely low SiO_2 content allows for the possibility of simultaneous production of both P_4 and CaC_2, which, while previously patented [18], would appear to be an untried processing route. If combined with acetylene production, e.g., for PVC manufacturing, flowsheet modeling indicates that the REE content of the concentrate would be increased in weight concentration by about 39%, *i.e.,* into an ~ 81 wt% $Ca(OH)_2$ residue with a 74% increase in REE content if calcined to CaO. A concentrate with such a weight concentration of REEs should be amenable to stockpiling (until another strategic REE supply crisis emerged) and subsequent hydrometallurgical processing. The economics of a combined pyrometallurgical process would be expected to be competitive in any location with low power cost, given the fact that both P_4 and CaC_2 are produced commercially using electric arc furnaces as the standard processing route.

Some of the thermodynamics of carbothermic reduction of fluorapatite concentrate are explored in Table 1 and Figs. 2, 3, and 4, all generated using HSC® version 7.1 and assuming ideal mixing at 1 atm pressure [19]. Figure 2 shows the equilibrium product distribution evaluated for a closed system at different temperatures, beginning with

Table 1 Some carbothermic reduction reactions of interest in the smelting of fluorapatite concentrate (where *Te* is the temperature of equilibrium under standard state conditions)

Reaction #	Reaction	$\Delta G^\circ = 0$ at °C	ΔH° kJ at T_e
(1)	$FeO + C = Fe + CO_{(g)}$	750	157.8
(2)	$KF + 0.5CaO + 0.5C = K_{(g)} + 0.5CaF_2 + 0.5CO_{(g)}$	1340	266.3
(3)	$NaF + 0.5CaO + 0.5C = Na_{(g)} + 0.5CaF_2 + 0.5CO_{(g)}$	1391	288.2
(4)	$MnO + C = Mn + CO_{(g)}$	1401	288.5
(5)	$Ca_5(PO_4)_3F + 7.5C + 9Fe = 0.5CaF_2 + 4.5CaO + 3Fe_3P + 7.5CO_{(g)}$	1411	2015.6
(6)	$Ca_5(PO_4)_3F + 7.5C + 6Fe = 0.5CaF_2 + 4.5CaO + 3Fe_2P + 7.5CO_{(g)}$	1448	2081.9
(7)	$Ca_5(PO_4)_3F + 7.5C + 3Fe = 0.5CaF_2 + 4.5CaO + 3FeP + 7.5CO_{(g)}$	1483	2284.8
(8)	$Ca_5(PO_4)_3F + 7.5C = 0.5CaF_2 + 4.5CaO + 1.5P_{2(g)} + 7.5CO_{(g)}$	1544	2690.6
(9)	$SiO_2 + C = SiO_{(g)} + CO_{(g)}$	1744	648.5
(10)	$CaO + 3C = CaC_2 + CO_{(g)}$	1826	458.2
(11)	$MgO + C = Mg_{(g)} + CO_{(g)}$	1845	605.4

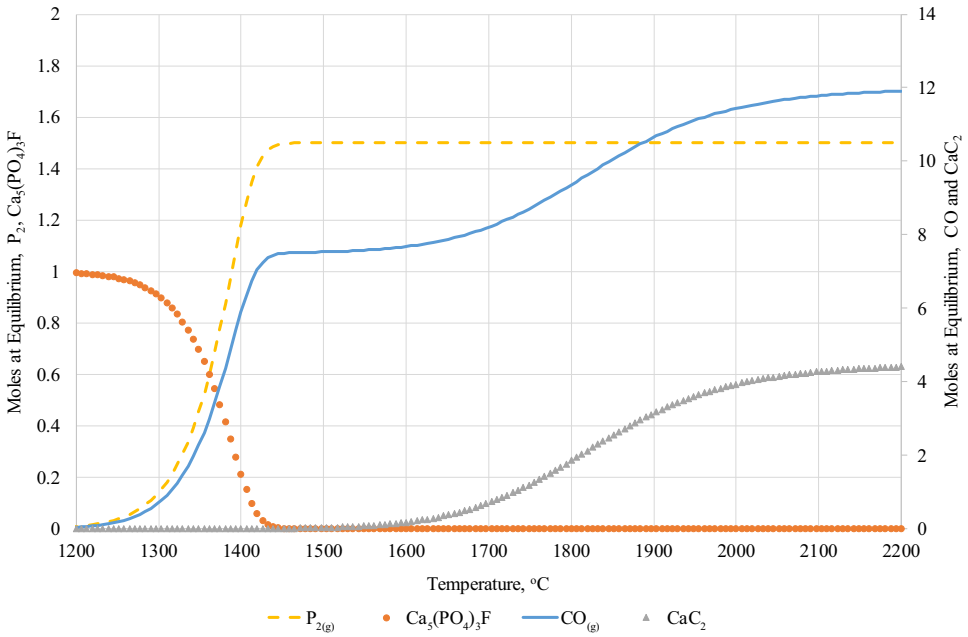

Fig. 2 Equilibrium amounts (arbitrary moles) for phosphorus extraction experiments conducted with excess C calculated using Equilibrium Calculations from HSC® version 7.1 [19], assuming ideal solutions, 1 atm total pressure, and a closed system (color figure online)

pure fluorapatite, with a large excess of carbon and without iron addition. Minor species actually present in the apatite concentrate have been eliminated for clarity, i.e., Na, K, etc.

Ideal solutions were assumed for the calculations as they are only intended to provide a rough indication over what temperature ranges reactions might take place, and what product species would be anticipated. A previously published evaluation of the $CaO–CaF_2$ system by Kim et al. [20] has shown it to be an ideal ionic solution, while other potential binaries, e.g., $CaF_2–Ca_3(PO_4)_2$, have shown heats of mixing [21], indicating that the assumption of ideal mixing introduces some errors to the results presented in Figs. 2, 3, and 4. More detailed modeling, using for example the integrated database computing system FactSage®, would potentially allow for better predictions if the required databases were commercially available. The standard FactSage® databases have already been shown to be insufficiently accurate for the high initial P_2O_5 content in apatite, and access is therefore required to a proprietary database [22]. Thermodynamic evaluations have been published in the literature on a number of binaries applicable to the experimental system [20, 23–25] forming a potential basis for more detailed future thermodynamic evaluations.

From Fig. 2, it can be seen that under equilibrium conditions significant amounts of P_2 and CO gas might begin to be produced at about 1200 °C and that under ideal

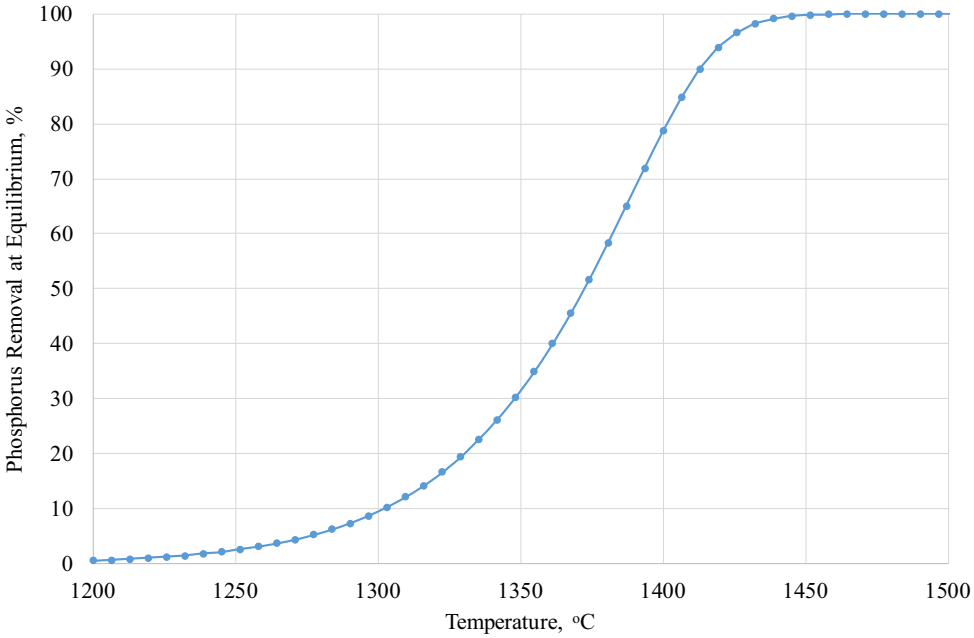

Fig. 3 Equilibrium phosphorus removal from apatite concentrate versus temperature calculated using Equilibrium Calculations from HSC® version 7.1 [19], assuming ideal solutions, 1 atm total pressure, and a closed system (color figure online)

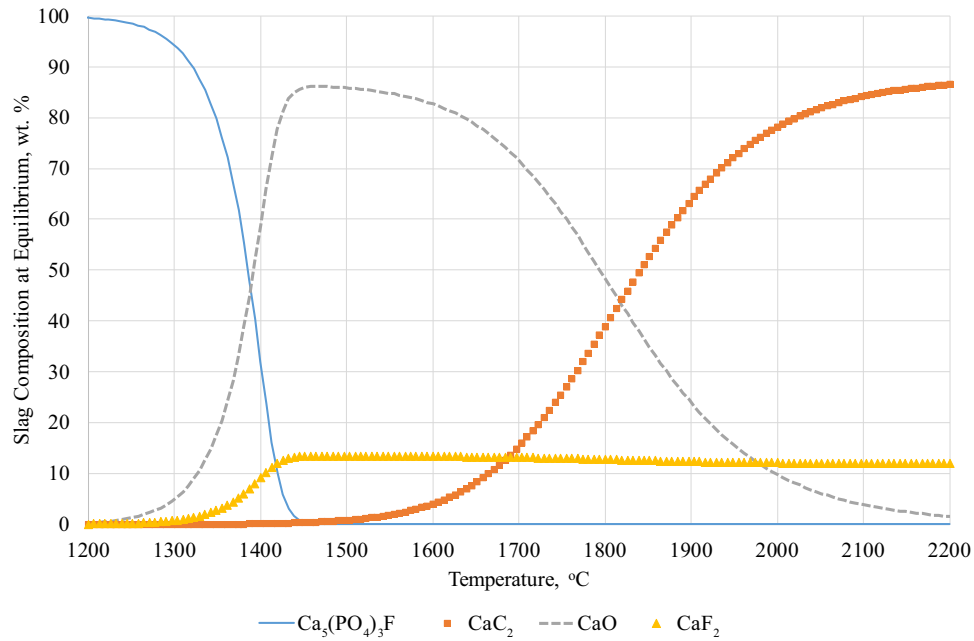

Fig. 4 Equilibrium carbide slag composition versus temperature with excess C calculated using Equilibrium Calculations from HSC® version 7.1 [19], assuming ideal solutions, 1 atm total pressure, and a closed system (color figure online)

conditions $Ca_5(PO_4)_3F$ would be fully consumed by a temperature of about 1450 °C, which would be the equivalent of complete phosphorus extraction as shown in Fig. 3. It can also be observed from Fig. 2 that CO gas generation from CaC_2 production would become significant at ~ 1550 °C.

As the melting range of the concentrate has already been shown in Part I of the present article to be about 1112–1613 °C, using TGA–DTA analysis, it was expected that the reaction rates for both reactions (8) and (10) accelerated once the fluorapatite became fully liquid. This would allow for an intimate contact between the liquid fluorapatite and the graphite crucible, which was the only source of reductant in the system. In addition, rapid removal of any residual phosphorus and production of carbide at temperatures exceeding ~ 1600 °C were expected, as the reaction rate for carbide formation (reaction 10) has been reported to only be significant over 1600 °C [26].

National standards exist for the quality of commercial grade CaC_2 expressed as *L* of acetylene per kg of product, and fall in the range of 260–300 L/kg [26]. Achieving these

standards necessitates a very high concentration of CaC_2, i.e., typically > 80 wt%, in the final product. The predicted product quality at equilibrium versus temperature is shown in Fig. 4, in the absence of silica, implying that an operating temperature of about 2000–2100 °C may be required in a commercial electric arc furnace process.

Industrially, the carbide production process is operated in the range of 1800–2100 °C [26]. Higher temperature operation allows for greater conversion of CaC_2 and easier tapping, due to the liquidus temperature in the CaC_2–CaO system, as shown in Fig. 5 for both technical and high purity grades. At equilibrium, the conversion of Ca contained in apatite to CaC_2 in the present experiments would be expected to achieve ~ 37% at 1800 °C, as indicated in Fig. 2. This would yield 46.6 wt% CaO, 40.7 wt% CaC_2, and 12.7 wt% CaF_2. Recalculating without CaF_2 yields 53.4 wt% CaO and 46.6 wt% CaC_2, and this composition of 'technical' grade CaC_2 would have a binary liquidus of about 1815 °C as indicated in Fig. 5. It would therefore be expected that a semi- or fully liquid slag product would be produced at experimental temperatures between 1800 and 1856 °C. CaF_2 formed by reactions (5–8), as well as NaF and KF (which are the more stable fluorides at lower temperatures), would likely improve the slag fluidity, as would minor contamination by other oxides present (see Part I of the present article—Tables 1 and 2 [13]) in the industrial concentrate used in these experiments.

A reduction in the levels of K, Na, Si, and Mg in the final product would be anticipated from reactions (2), (3), (9), and (11), respectively. In addition, transition metals such as Fe and Mn would be expected to be present predominantly in a metal phase, as indicated by reactions (1) and (4). The metallic product would be expected to be primarily an alloy of Fe and P, i.e., ferrophosphorus.

The thermodynamics of the standard carbide production process have been described in some of the limited information that is available in the literature [28, 29].

Apparatus and Procedures

Phosphorus removal experiments were performed in a vacuum furnace operated under approximately atmospheric conditions (~ 0–30 millibars gauge pressure) using a steady purge of 9.44 L/min (20 SCFH) 4 N purity argon, as shown schematically in Fig. 6. A series of 14 experiments were performed during which the apparatus and procedures evolved as operational experience was gained. The final procedure is described, which correspond with the results to be presented in the present study.

In the current experiments, the production of P_2 gas (and ultimately P_4 condensate) was initially considered a safety hazard, due to its tendency to both spontaneously combust in air and its proclivity to produce toxic PH_3 gas if sources of 'caustic' and water are available. Therefore, a large excess (6:1 mass ratio) of iron was initially used in an attempt to absorb as much as possible the P_2 gas produced in the reduction crucible. According to thermodynamic analysis, only FeP and Fe_2P should have been produced under the applied experimental conditions, i.e., at about 1800–1860 °C; however, in reality 40% of the phosphorus reported to the gas phase, 59% to the metal phase, and 1% to the slag phase, which did not eliminate any risks. Obviously, the presence of iron on the bottom of the crucible was insufficient to ensure complete absorption, i.e., as

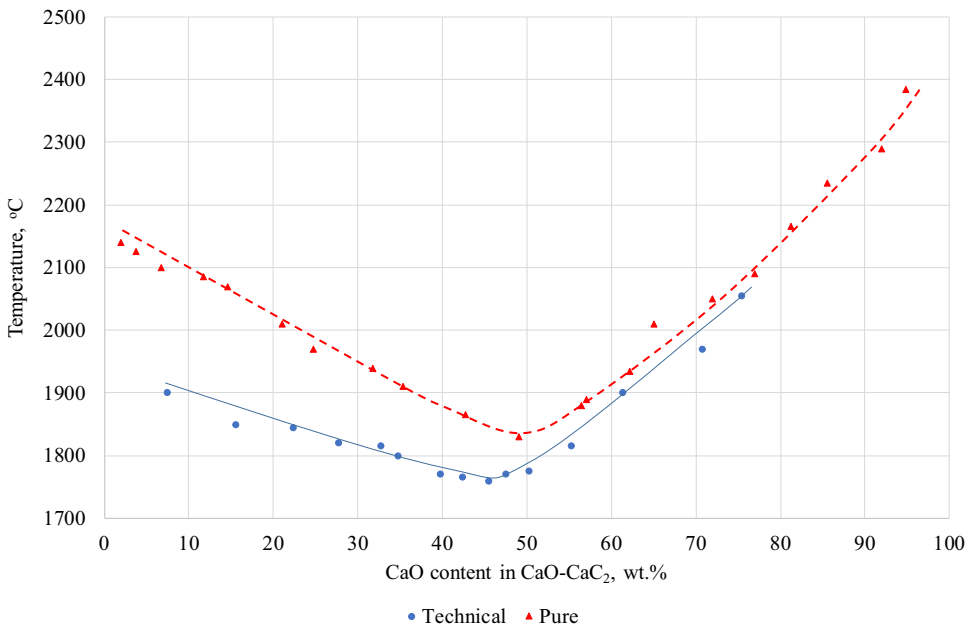

Fig. 5 Binary phase diagram for CaO–CaC_2 using **a** "technical" grade CaC_2 and **b** chemically pure CaC_2 [27] (color figure online)

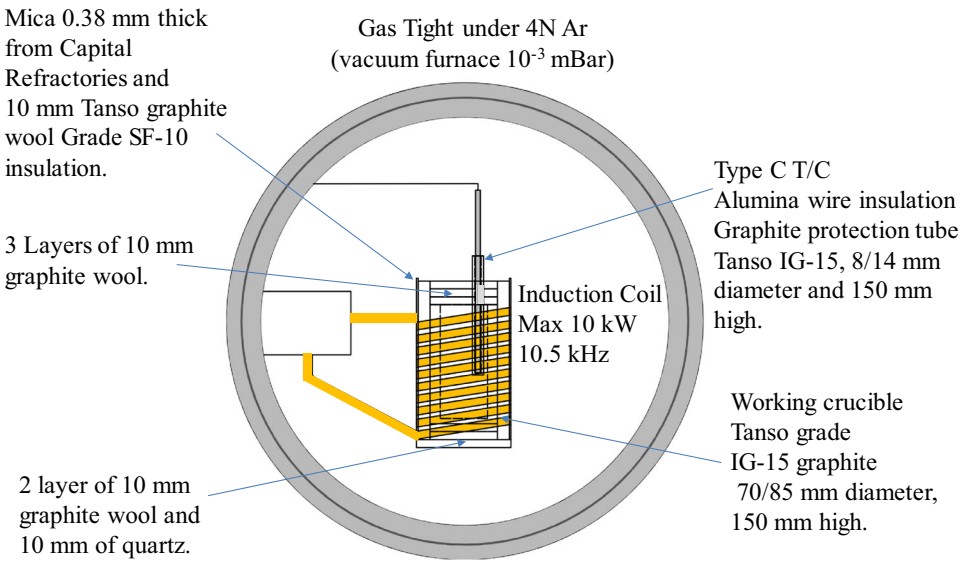

Fig. 6 Experimental apparatus for phosphorus removal experiments (color figure online)

FeP, Fe_2P, and Fe_3P, of the highly volatile phosphorus. It was later decided to eliminate the use of iron, once the safety procedures regarding P_2 and PH_3 were fully established. The test results obtained from the experiments without iron are therefore reported.

50 g of the apatite concentrate was pre-calcined at 1000 °C for one hour in order to remove CO_2 and prevent damage to the graphite wool insulation from the Boudouard reaction. The crucible was loaded with the concentrate, the furnace immediately sealed and evacuated down to 10^{-3} mBar, after which it was filled and continuously purged with 4 N argon. 2 kW was applied to the induction coil using a 10.5 kHz power supply. The power was increased at 0.5-kW increments at fixed intervals, using the furnace controller, up to a maximum of 3.5 kW. The furnace operating pressure was monitored throughout the experiment, and the flow of argon was controlled to a constant rate. The final experiments were operated for $\sim$ 130 min, of which the final 30 min were at an average temperature of $\sim$ 1855 °C. The temperature was measured by a type C thermocouple located inside the crucible and protected by an alumina inner and graphite outer protection tube. In some experiments, a second type C thermocouple was placed bare into the freeboard to give an additional and faster responding reading. The freeboard thermocouple did, however, tend to fail, and since it gave substantially the same readings as the sheathed thermocouple, its use was discontinued.

At the end of the experiments, the furnace was cooled under argon and later air, when the crucible contents had reached $\sim$ 400 °C, in order to combust any P_2 that had been released during the reactions. The furnace was held under air for $\sim$ 16 h before opening and cleaning. Excellent ventilation, a gas sampling apparatus, as well as appropriate respirators for PH_3 gas, were used during the post-experimental handling of samples.

Results and Discussion

Experimental Results

A typical experimental temperature and pressure versus time curve is presented in Fig. 7. As the argon gas flow was held constant at 9.44 N L/h, the variation of the reactor back pressure versus time (due to the presence of an outlet valve and gas line) is indicative of the changes in the volume of gas produced at any given time, with the ΔP being approximately proportional to the flow squared (and ignoring minor compressibility effects).

The formation of P_2 gas was clearly observable from the furnace viewing port during the experiments. P_2 gas condensed into a visible P_4 plume upon exiting the hot reactor into the cold chamber of the sealed vessel. Initial signs of vapor production were observed beginning at about 1300 °C, in accordance with the thermodynamic predictions shown in Figs. 2, 3, and 4; however, significant quantities of vapour were present only from $\sim$ 35 min into the test, at a measured temperature of 1506 °C, and until $\sim$ 105 min into the test, and a temperature of 1854 °C, for the experiment shown in Fig. 7. Visually, the peak of the vapour production was observed at 75 min and 1805 °C, which corresponded to a significant change in the pressure curve as shown in Fig. 7. CO gas continued to be produced in the absence of a visible vapour stream, due to the formation of CaC_2 according to reaction (10), and as indicated in Figs. 2 and 4, until the experiment was terminated.

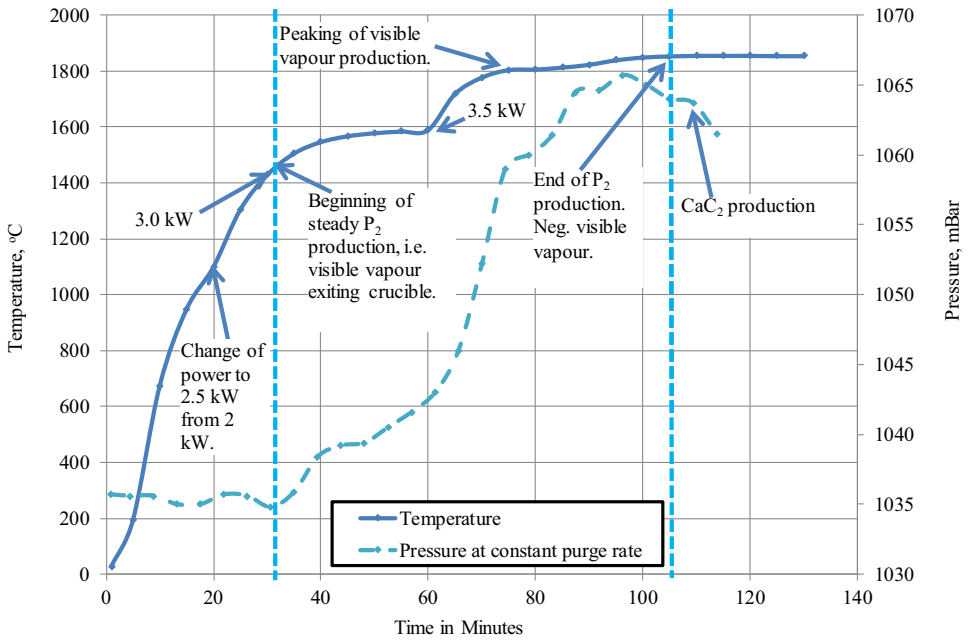

Fig. 7 Dephosphorization experimental temperature and pressure versus time (color figure online)

The results presented in Fig. 7 appear to confirm that while reduction reactions could take place before the melting of the apatite, they were greatly accelerated after complete melting, i.e., > 1613 °C as previously reported in Part I of the present article, and as indicated by the pressure curve. The P_2 production continued to higher temperatures, i.e., > 1800 °C, than what was expected from a strictly thermodynamic perspective (< 1450 °C as indicated in Fig. 3). Overall, the 'dual wave' of the CO gas production, as predicted in Fig. 2, was observed experimentally, but shifted to higher temperatures than expected from the simplified thermodynamic assessment. Intimate mixing of concentrate and reductant would be expected to increase rates of reaction and lead to greater phosphorus removal at lower temperatures. In these experiments, the only reductant present was the graphite crucible itself, and intimate contact could only be achieved after melting of the apatite concentrate.

After partially cooling the reactor, air was allowed into the vessel, which then ignited the condensed P_4 and spontaneously produced a large opaque white cloud of P_2O_5. The vessel was held with an air atmosphere for 16 h, after which the vessel was opened. PH_3 in toxic quantities (in the absence of personal protective gear or adequate ventilation) was found to immediately begin to form when the vessel contents were exposed to laboratory air containing a normal moisture content. A full-face respirator was used to transfer the graphite crucible to a fume hood, where the contents of the crucible were reacted with water, producing vigorous bubbling from C_2H_2 formation and substantial (toxic) quantities of PH_3 over a period of about 2–3 h. Representative images of the obtained product prior to reaction with water are presented in Fig. 8, clearly indicating melting and conversion of the initial powdered raw material. It was not deemed safe to handle the samples

Fig. 8 Representative photographs of the solidified CaC_2-containing slag: (left) in the bottom of the graphite crucible and (right) removed prior to reaction with water to produce C_2H_2 and PH_3 (color figure online)

prior to elimination of the PH_3, and analyses were therefore not performed on the 'as-produced' product prior to reaction with large quantities of water.

After at least 24 h under water, the graphite crucible contents were vacuum filtered through standard #4 filter paper, dried, and calcined at 1000 °C prior to chemical analyses being made via Inductively Coupled Plasma Mass Spectrometry (ICP-MS). The averaged chemical analyses are presented in Table 2 for both the initial and the final nearly phosphorus-free residue, which was calcined prior to analysis to remove hydrated water. Up to 7 apatite concentrate raw material assays from 3 different laboratories were averaged, as previously presented in Part I of the present article—Table 2. The product results, i.e., slag and ferrophosphorus, presented in Table 2 are the average of 2 experimental results where melting or partial melting of the product was achieved. Ratios have been calculated between the final slag and the initial concentrations of the apatite concentrate to show the impact of the removal of CO_2, phosphorus, and oxygen on the final concentration of the REEs. The assays of the small quantity of FeP produced are also indicated.

The final masses of slag and ferrophosphorus can be estimated from the assays in Table 2, by assuming that the Ca is present in the slag/salt phase and that all Fe not present in the slag phase is found as ferrophosphorus. This reveals that 50 g of apatite concentrate will produce 28.9 g of final calcined slag, i.e., CaO not $Ca(OH)_2$, and 0.62 g of ferrophosphorus. The balance of the mass, i.e., 20.5 g, is assumed to have reported to the gas phase during the pre-calcination step, as well as during the final reaction. The two products could not be fully removed from the crucible, and they could not be easily separated (this is especially true for the small ferrophosphorus particles dispersed in the slag phase). The material lost to the gas phase could not be monitored in the vacuum induction furnace apparatus used in the present experiments.

Weighing and analyses of the slag prior to reaction with water were not made, due to its tendency to release highly toxic PH_3. X-ray powder Diffraction (XRD) analysis was therefore performed on the slag in its hydrated form, and the obtained results are included in Fig. 9, where they are compared with the original apatite concentrate spectrum. The XRD results indicate that the original minerals have been converted to hydrated lime, $Ca(OH)_2$, calcium fluoride silicate, $Ca_{6-0.5x}Si_2O_{10-x}F_x$, aluminum phosphide, AlP, and calcium yttrium oxide, $Ca_{0.84}Y_{0.1}O$.

As shown in Fig. 9, the XRD patterns presented for the apatite concentrate before and after dephosphorization indicate a complete change in the phases present. Calcite decomposed into CaO, which subsequently reacted to CaC_2 (the presence of CaC_2 being indicated by strong bubbling when contacted with water), before being

Table 2 Comparison of apatite concentrate (see Part I of the present article—Table 2 for further details) and average results of de-phosphorized slag and ferrophosphorus assays from experiments conducted at a maximum temperature of 1856 °C (1 SD is indicated where multiple assays are available)

Results in ppm	P	Na	K	Mg	Si	Al	Ca	Mn
Apatite	140,857 ± 6543	2636 ± 1752	443 ± 336	7786 ± 726	6733 ± 1537	1313 ± 450	356857 ± 16618	1504 ± 136
De-P slag	659 ± 315	<200	<200	5368 ± 1873	16519	1876 ± 229	689,668 ± 48334	579 ± 65
Ratio	*0.0047*	*<0.08*	*<0.45*	*0.69*	2.47	1.43	1.93	**0.39**
Ferrophosphorus	178,463 ± 26387 ±315	<100	<100	259 ± 100	2102 ± 494	529 ± 364	1 ± 0	34,188 ± 11260
Results in ppm	Fe	Ti	Y	Ce	La	Nd	Dy	Pr
Apatite	10,900 ± 1375	560 ± 62	590 ± 26	1865 ± 68	840 ± 41	808 ± 41	82 ± 14	187 ± 25
De-P slag	2275 ± 136	1359	1036 ± 66	3442	1593 ± 80	1817 ± 276	135 ± 77	408
Ratio	**0.21**	2.43	1.76	1.85	1.90	2.25	1.65	2.18
Ferrophosphorus	Balance	N/A	66 ± 13	1280 ± 447	463 ± 239	915 ± 299	19 ± 3	20 ± 5

Items marked in italics have evaporated, in bold reported to the metal phase, and in black primarily to the slag phase

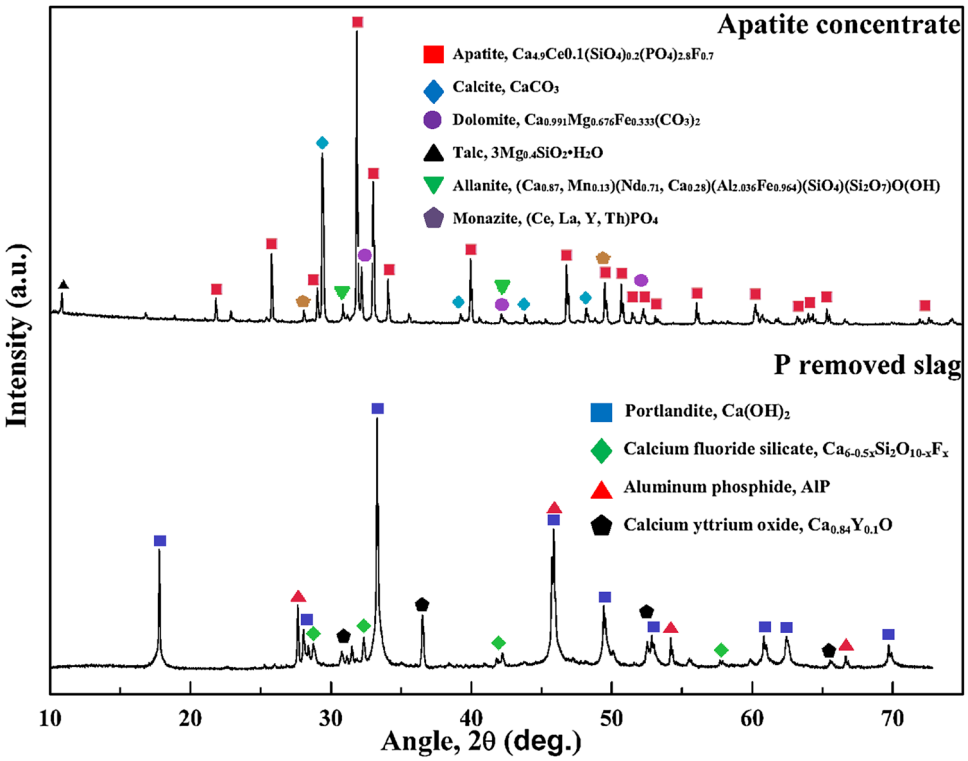

Fig. 9 XRD results from using a powder diffractometer (Bruker D8 Advance A25) operating in Bragg–Brentano mode, and utilizing Cu K-alpha radiation. A 2θ range of 10°–75° using a voltage of 30 kV. The collected data were analyzed using the software DIFFRAC.EVA V3.0 from Bruker with the database PDF-4+2013 RDB (color figure online)

converted to $Ca(OH)_2$ due to hydration. It is also noteworthy that the MgO species is no longer detectable (an estimated 56% has reported to the gas phase). The three main REE-containing phases restructured into different phases including calcium fluoride silicate and calcium yttrium oxide. In addition, there were additional phases produced such as aluminum phosphide (AlP), which was likely the source of P leading to PH_3 creation (in addition to the P from the ferrophosphorus).

Due to the presence of both CaF_2 and rare earth-containing silicates in the lime residue, it is anticipated that aggressive methods such as the roast–leach method, applied to bastnasite, may be required [30] to achieve adequate recovery of REEs, which is primarily a result of the extremely low solubility of rare earth fluorides [31].

The data in Table 2 indicate that the majority of the potentially volatile species identified in Table 1 have vaporized to a substantial degree based on the observed and estimated ratios between the final and the initial assays, i.e., P (0.0047), Na (< 0.08), K (< 0.23), and Mg (0.69). The REEs have been concentrated in the final calcined residue by an average factor of 1.9, which slightly exceeds the expected ratio of 1.7 for the calcined product, i.e., the assays in Table 2 are for a slag containing CaO and not $Ca(OH)_2$). The Fe and Mn present have both been concentrated into the ferrophosphorus phase.

Industrial Implications

Mass and energy balances were prepared for an envisaged electric furnace process similar to the one previously depicted in Fig. 1 and designed to maximize value recovery from the apatite concentrate, i.e., recovery of the value of the phosphorus content. By the use of higher temperatures than the standard phosphorus process, the new proposed process would simultaneously produce calcium carbide and allow the REE content of the concentrate to be recovered later after conversion of carbide to acetylene. One key objective of the proposed process was to avoid destruction of the REE value present in the raw material.

Using the pilot apatite concentrate assay reported in Part I of the present article, and a petroleum coke assaying, i.e., 86.7% C, 3.64% H, 3.2% O, 1.59% N, and 4.9% S, the mass and energy balances were calculated using Metsim®, a flow sheet simulation program [32]. It was assumed that the calcite and dolomite were fully calcined in the sintering kiln. It was further assumed that the calcine could be fed hot to the electric smelting furnace at 700 °C, which has good precedent from the FeNi industry where hot calcine is routinely transported in insulated containers and used at temperatures from 700 to 900 °C at the furnace.

It should be noted that the combined P_4/CaC_2 process has a great deal of chemical energy and sensible heat available in the off-gas, due to the additional volume of CO gas produced during carbide making (over the P_4 process

Table 3 Indicative mass and electrical energy requirement for P_4 [3], CaC_2 [26], and combined P_4/CaC_2 processes

Product	Raw material	Mass of feed (kg)	Reductant (kg)	Flux (kg)	Power (kWh/mt of feed)	Products		By-product FeP (kg)
						P_4 (kg)	CaC_2 (kg)	
P_4	Phosphate	1000	156	350	1625	125	0	15
CaC_2	Calcined lime	1000	579	0	3263	0	1053	0
P_4/CaC_2	Apatite	1000	617	0	2957+	136	642	12.3

+ Based on a theoretical mass–energy balance performed using the process simulation system Metsim®, and assuming a 92% furnace thermal efficiency

alone). The off-gas energy content is, in other words, sufficient to calcine the feed, sinter the pellets, and preheat the feed; hence, a reduced furnace electrical energy consumption can be achieved. The cooling step, depicted in Fig. 1 after the sintering kiln, is therefore not required if a high-temperature handling system for solids is utilized. In addition, the final off-gas from the calcining process contains an additional energy content above what is required to calcine, sinter, and preheat the feed, of 2.9 MW/mt of the concentrate processed, allowing for further energy recovery and/or integration.

The typical reductant, flux, and furnace energy usage per tonne of feed are indicated in Table 3 for the phosphorus, carbide, and combined processes. Product and by-product masses are also indicated. From Table 3, it is clear that the combined reduction process is highly endothermic, and it was estimated that 2957 kWh/mt would be required to produce 79.0% CaC_2 at 2050 °C, which should be sufficiently fluid for tapping according to Fig. 4 [27]. This energy consumption assumed an off-gas temperature of 727 °C [29], and a typical large-scale, e.g., 50 MW, furnace with a thermal efficiency of about 92%.

Assuming a P_4 furnace energy consumption of only 13 MWh/mt of P_4 [3] and taking credit for 211 kg of P_4 produced per tonne of 79.0% CaC_2 would yield a net consumption of only 1.85 MWh/mt of technical grade CaC_2 (with a quality of 276 L of acetylene per kg), which is well below the values typically achieved by ordinary carbide producers, i.e., 3–3.3 MWh/mt [26]. These results indicate that the electricity consumption of such a combined process would compete positively with existing practices, and that the process would have a good probability of being economical if technically viable at a large scale.

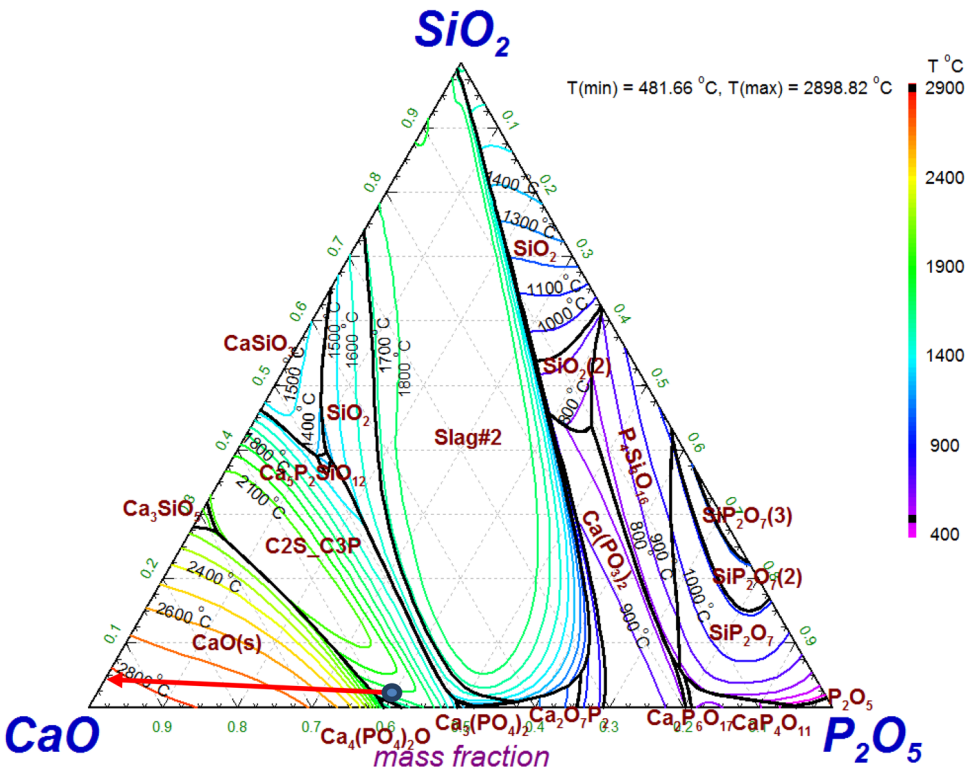

Fig. 10 $CaO–SiO_2–P_2O_5$ phase diagram indicating the increase of liquidus in the absence of silica fluxing and carbide production, and with the removal of phosphorus. The blue dot indicates the initial composition of the apatite concentrate [12] (color figure online)

It is interesting to note that one experiment was performed where the slag remained a powder and a final solid with 2.0% P was obtained, i.e., > 87% P removal based on a mass balance. Even though the same power profile was applied as in the successful experiments, the indicated temperature never increased beyond 1697 °C, which is likely due to the insulating behavior of the high-lime product. The path from low silica apatite toward phosphorus-free slag is presented in Fig. 10, showing the monotonic increase in liquidus temperature with the degree of phosphate removal in the absence of carbide formation. As shown in the figure, it is obvious that if phosphorus can be removed rapidly enough at temperatures below the melting point of apatite, that melting can be avoided even at very high operating temperatures and degree of phosphorus removal, due to the extremely high CaO content of the product.

In theory, full phosphorus removal can be achieved at 1450 °C, as previously indicated in Fig. 3, in the absence of melting. To achieve this objective, an intimate mixing of reductant and concentrate would be required to produce a self-reducing pellet, very similar to those produced in the IHP [6, 7]. Unlike the IHP, it is not required (at least in theory) to use silica. In fact, it would appear according to Fig. 10 that silica additions could be counterproductive producing a lower melting product and resulting in kiln build-up, i.e., 'ringing'. The use of silica would also result in lower REE assays in the final residue. Operating the reduction process without silica would require somewhat higher temperatures than the 1280–1340 °C currently applied [7] in the IHP process, which would result in slightly higher energy consumption than the version of the process now being demonstrated. However, as the IHP process uses in situ re-combustion of P_2 to P_2O_5 in the gas phase of the kiln, i.e., an oxidizing atmosphere over the hot bed of self-reducing pellets, and counter-current transfer of energy to the incoming charge, the increase in total energy consumption would be expected to be minimal.

Conclusions

It has been shown to be possible to simultaneously produce phosphorus and a calcium carbide slag at 1856 °C that contains substantially all of the REEs, i.e., ~ 99.7% by weight, of what was present in the raw material (in the present case a pilot apatite concentrate). The REE content in the final slag was enriched by more than 90% from the initial mass concentration in the apatite concentrate. The resulting lime residue enriched in REE can be stockpiled and further treated for their recovery when the economics of this market become favorable.

Energy consumption for a combined process to produce P_4 and CaC_2 simultaneously from apatite is theoretically superior to the current commercial results for an equivalent CaC_2 production process, indicating a net reduction of about 40% after credits for P_4 production.

The possibility for a 'dry' process to produce P_2O_5 without the use of silica flux was identified, potentially allowing for further enhancement of the IHP.

Future Work

Phosphorus-'free' residue produced by the carbothermic reduction of the pilot apatite concentrate presently investigated will be processed hydrometallurgically to characterize its leaching behavior with respect to the sought-after REO minerals. A value chain analysis of the envisaged integrated process will, based on this, be presented in a future paper describing the total operating cost and value generation beginning with mineral processing and finishing with the post-treatment of the residue.

Acknowledgements The authors would like to thank their co-participants in this EU-funded project (Grant FP7-603564—REE-cover) for their assistance in performing the present work. Thanks are given to J.R. Tolchard for help during the XRD analyses and D. Slizovskiy for experimental assistance. The second author would also like to thank the Chinese Scholarship Council (CSC) for funding his PhD research.

References

1. Schipper W, Klapwijk A, Potjer B, Rulkens W, Temmink B, Kiestra F et al (2001) Phosphate recycling in the phosphorus industry. Environ Technol 22:1337–1345
2. Schipper W (2014) Phosphorus: too big to fail. Eur J Inorg Chem 2014:1567–1571
3. Diskowski H, Hofmann T (2000) Phosphorus: Ullmann's encyclopedia of industrial chemistry. Wiley-VCH Verlag GmbH & Co., New York, pp 725–746
4. Scheepers E, Yang Y, Adema AT, Boom R, Reuter MA (2010) Process modeling and optimization of a submerged arc furnace for phosphorus production. Metal Mater Trans B 41:990–1005
5. Schorr M, Valdez B, Zlatev R, Stoytcheva M (2010) Phosphate ore processing for phosphoric acid production: classical and novel technology. Min Process Extr Metal 119:125–129
6. Anonymous (2014) Fertilizer Focus:A-D
7. Walters M (2011) A technical review of the improved hard process. Presented at the international technical conference, New Delhi, India, pp 1–13

8. Frietsch R, Perdahl J-A (1995) Rare earth elements in apatite and magnetite in Kiruna-type iron ores and some other iron ore types. Ore Geol Rev 9:489–510
9. Pålsson BI and Fredriksson A (2012) Apatite for extraction. II. Flotation of apatite and rare earth elements from old tailings dumps. XXVI international mineral processing congress (IMPC) 2012, New Dehli, India, pp 04064–04075
10. Pålsson BI, Martinsson O, Wanhainen C and Frederiksson A (2014) Unlocking rare earth elements from European apatite-iron ores. In: Proceedings 1st European rare earth resources conference (ERES2014), pp 211–220
11. Wanhainen C, Pålsson BI, Eriksson AE (2016) New REE mineralogy for LKAB apatite-iron ORES. Presented at mineral Teknik 2016, pp 1–16
12. http://www.reecover.eu/. Accessed 22 Nov 2016
13. Sun T, Kennedy MW, Yurramendi L, Aldana JL, Del Rio C, Arnout S, Tranell G and Aune RE (2017) Pyrometallurgical treatment of apatite concentrate with the objective of rare earth element extraction: part I. J Sustain Metal. https://doi.org/10.1007/s40831-017-0140-6
14. Sun T, Kennedy MW, Tranell G, Aune RE (2015) Apatite concentrate, a potential new source of rare earth elements. In: Neelameggham NR, Alam S, Oosterhof H, Jha A, Dreisinger D, Wang S (eds) Rare metal technology 2015. Springer, Cham, pp 145–156
15. Wang Z, Jiang M, Ning P, Xie G (2011) Thermodynamic modeling and gaseous pollution prediction of the yellow phosphorus production. Ind Eng Chem Res 50:12194–12202
16. E.U. Commission (2014) Report on critical raw materials for the EU:1-41
17. Karshigina Z, Abisheva Z, Bochevskaya Y, Akcil A, Sargelova E (2015) Recovery of rare earth metals and precipitated silicon dioxide from phosphorus slag. Miner Eng 77:159–166
18. Jonas K (1958) Process for production of calcium carbide and phosphorus. Patent US2860037
19. http://www.outotec.com/en/Products–services/HSC-Chemistry/Calculation-modules/Sim–process-simulation/. Accessed 15 Sept 2015
20. Kim DG, Van Ende MA, van Hoek C, Liebske C, van der Laan S, Jung IH (2012) A critical evaluation and thermodynamic optimization of the CaO-CaF_2 system. Metal Mater Trans B 43:1315–1325
21. Tacker R, Stormer J (1993) Thermodynamics of mixing of liquids in the system $Ca_3(PO_4)_2$–$CaCl_2$–CaF_2–Ca $(OH)_2$. Geochim Cosmochim Acta 57:4663–4676
22. Arnout S, Nagels E (2016) Modelling thermal phosphorus recovery from sewage sludge ash. Calphad 55(Part 1):26–31
23. Lindberg D, Chartrand P (2009) Thermodynamic evaluation and optimization of the (Ca + C+O + S) system. J Chem Thermodyn 41:1111–1124
24. Serena S, Carbajal L, Sainz MA, Caballero A (2011) Thermodynamic assessment of the system CaO–P_2O_5: application of the ionic two-sublattice model to glass-forming melts. J Am Ceram Soc 94:3094–3103
25. Hudon P, Jung IH (2015) Critical evaluation and thermodynamic optimization of the CaO-P_2O_5 system. Metal Mater Trans B 46:494–522
26. Langhammer B (2002) Calcium carbide. Ullmann's encyclopedia of industrial chemistry, pp 1–14
27. Juza R, Schuster HU (1961) Das Zustandsdiagramm Calciumcarbid/Calciumoxyd. Z Anorg Allg Chem 311:62–75
28. Ji L, Liu Q, Liu Z (2014) Thermodynamic analysis of calcium carbide production. Ind Eng Chem Res 53:2537–2543
29. Healy G (1995) The calculation of an internal energy balance in the smelting of calcium carbide. J S Afr Inst Min Metall 95:225–236
30. Kul M, Topkaya Y, Karakaya I (2008) Rare earth double sulfates from pre-concentrated bastnasite. Hydrometallurgy 93:129–135
31. Chi R, Zhang X, Zhu G, Zhou ZA, Wu Y, Wang C et al (2004) Recovery of rare earth from bastnasite by ammonium chloride roasting with fluorine deactivation. Miner Eng 17:1037–1043
32. Kennedy MW (2014) Metallurgical plant optimization through the use of flowsheet simulation modelling. In: Celebrating the megascale: proceedings of the extraction and processing division symposium on pyrometallurgy in honor of David GC Robertson. The Minerals, Metals & Materials Society, Warrendale, pp 367–375